J Mater Sci: Mater Med (2010) 21:1385–1392
DOI 10.1007/s10856-009-3946-3

Random damage and characteristics of debris particles are two important and yet ignored factors in the mechanical integrity of the stem-cement interface of a total hip replacement: influence of the surface finish of the metal stem

Gang Qi · Steven F. Wayne · Kenneth A. Mann · Bin Zhang · Gladius Lewis

Received: 1 May 2008 / Accepted: 16 November 2009 / Published online: 28 November 2009
© Springer Science+Business Media, LLC 2009

Abstract The importance of the conditions at the stem-cement interface in cemented total joint replacements (THRs) with regard to the in vivo longevity of the implant is well recognized. In the present study, we used a simplified model of one part of a cemented THR (alloy rectangular beam bonded to rectangular cement plate) to study the influence of surface finish of the alloy beam (stem) on two measures of the evolution of random damage at the alloy beam-cement plate interface (stem-cement interface), under quasi-static direct shear load. Three surface finishes of the beams were used: satin-finish, grit-blasted, and plasma-sprayed. The random damage events were monitored from the emitted acoustic signals, with the two measures computed from these signals being the intensity of random damage events (IRDE) and the mean damage event energy (MDEE). Large number of random damage events (higher values of IRDE and low value of MDEE) occurred with grit blasted specimens, suggesting a high probability for the generation of debris particles at the interface. These findings, in conjunction with details on the size and shape of the debris particles, obtained using scanning electron microscopy, lead to the suggestion that satin-finish stems are desirable for use in cemented THRs.

G. Qi (✉) · S. F. Wayne · B. Zhang · G. Lewis
Department of Mechanical Engineering, The University of Memphis, Memphis, TN 38152, USA
e-mail: gangqi@memphis.edu

K. A. Mann
Department of Orthopedic Surgery, Upstate Medical University, Syracuse, NY 13210, USA

1 Introduction

It is well known that aseptic loosening is the most common reason for the revision of total joint replacements [1]. In the case of cemented total hip replacements (THRs), it has been postulated that bonding conditions at the stem-cement interface play a critical role in aseptic loosening of the implant [2–6]. Among the factors that influence these conditions are the polymerization front of the curing cement [3, 7, 8], the viscosity of the curing cement [9], and the surface roughness of the stem [3, 10–13]. Much research attention has been paid to the surface finish of the stem, from polishing the stem to prevent bonding, to roughening the stem surface to create an interlocking mechanism between stem and the cement, to precoating the stem with a layer of the cement are all approaches used clinically to achieve optimal stem-cement interface conditions [14–16]. The clinical evidence on the influence of stem surface finish on the in vivo longevity of cemented THRs is far from clear, with, for example, conflicting reports regarding roughened versus smooth (polished or satin finish) stems [17–22]. There is consensus, however, on another aspect of the stem-cement interface, which is that the cemented THR is likely to have a poor outcome if the stem-cement interface fails via the generation of debris particles secondary to the failure of the interface. It has been suggested that this production could be minimized by improving the bonding conditions at the stem-cement interface through, for example, increasing the interface shear strength [1, 4, 9, 12]. The rationale for this suggestion is that the generation of debris particles would be limited if the interface bonding is strong enough to maintain integrity for the lifetime of the implant [23]. Although there is a substantial body of literature that indicates that a rough stem interface more likely to fail than a smooth interface

[24], little is known about the this interface under the influences of naturally occurred random damage events, and the morphology of debris particles due to these events at the stem-cement interface under physiologically relevant loading conditions.

To measure these random damage events, in the present work, we used a non-invasive technique to quantify the intensity and the energy of each damage event in a simplified model of stem-cement interface under quasi-static shear loads. We also characterized the debris particles produced at this interface. We hypothesized that: (1) the major failure mechanism at smooth interface is interface debonding, whereas that at rougher interface is dominated by the breakage of interlocked cement fragments; (2) stem surface random damage events initiate at very low stress levels, and, hence, establish the basis for microstructural damage and subsequent debris formation.

2 Materials and methods

2.1 Fabrication of test specimens

Thirty-one CoCr alloy solid rectangular bars with nominal dimensions of 5.9 mm × 11.1 mm × 63.0 mm and three different surface finishes, namely, satin-finish, grit-blasted, and plasma-sprayed, were prepared for this study. These finishes represent the range that has been used in stems in cemented THRs. We did not include polished surface because it is widely assumed that polished stems do not lead to mechanical bonding at the stem-implant interface in cemented THRs [16, 25]. Ten alloy bars were blasted with glass beads (satin-finish group), twelve were grit blasted with 16-grit alumina (grit-blasted group), and nine were plasma sprayed (plasma-sprayed group). The arithmetic-average surface roughness (R_a) of each beam was measured using a contact profilometer (Surfcom 1800D, Zeiss GmbH, Germany) with a travel length and cutoff length of 15 mm and 5 mm, respectively.

We deposited a thick layer of a poly (methyl methacrylate) (PMMA) bone cement (VersaBond^{TM}; Smith & Nephew, Inc., Memphis, TN) on top of the alloy beams in the following manner. The cement powder and liquid monomer were mixed, at between 1 and 2 Hz, in a polymeric bowl open to the ambient laboratory atmosphere (temperature and relative humidity of 22 ± 1°C and 56 ± 2%, respectively) for 30–40 s. The beams were placed in a rectangular mold after which the cement dough was poured into the mold. The cement was allowed to cure for at least 48 h before the beams were removed from the mold and then their edges were sanded to remove excess cement. We thus obtained a simplified model of the stem-cement interface (Fig. 1).

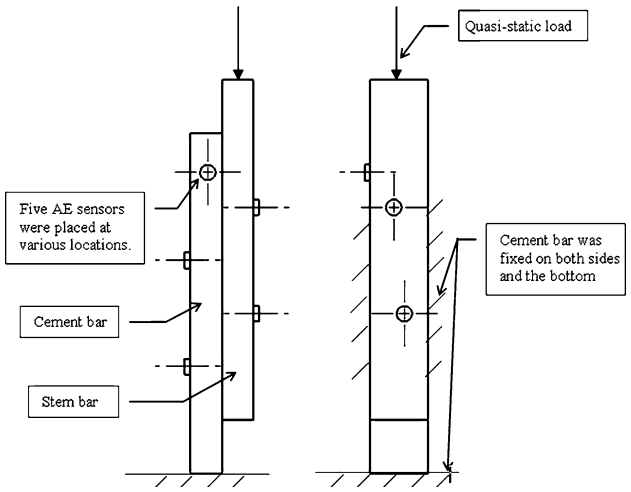

Fig. 1 Schematic drawings of the test specimen

2.2 Acoustic emission tests

In these tests, a direct shear force was applied using a screw-driven materials testing machine (Model 4465; Instron Corp., Canton, PA), at a crosshead displacement rate of 1 mm/min. The acoustic emission (AE) signals were monitored using five sensors (Nano 30, Physical Acoustics, Inc., Princeton, NJ) that were glued to the specimen surface. The acquired AE signals were conditioned first by preamplifiers (AEP4, 40 dB, Vallen-Systeme GmbH, Germany) and then fed to a multi-channel AE system (ASMY-5, Vallen-Systeme GmbH, Germany). The apparent shear strength of the alloy plate-PMMA bone cement layer interface (τ_s) was obtained by dividing the applied force by the area of the interface. The stress ratio (SR) was computed as the ratio of the stress at the onset of random damage events (τ_o) to τ_s. SR may also be thought of as the relative onset stress.

In order to examine the random damage produced in early loading, we divided the loading sequence into three stages: pre-yield, yield, and post-yield. The pre-yield stage is defined as the zone between the acoustic signals onset point and the point where the applied load reaches 90% of its maximum value (hereafter called the 90% load point). This onset point is indicated when AE signals become substantial (a sudden change in the slope of the plot of AE signals versus load). The damage events occurring in the pre-yield stage are referred to as pre-yield events. The yield stage is defined as the zone between the 90% load point and the point where the load slightly passes the ultimate load. The damage events occurring in this stage are referred to as yield events, and those occurring after the yield stage are called post-yield events. We did not use peak load as the 'yield' point because it was apparent that yielding occurred before the peak load was reached. In this

Table 1 Characteristic indication of random damage by the combination of IRDE and MDEE

	Small IRDE	Large IRDE
Large MDEE	Large physical scale of random damage events with large event energy	Both physical scale and quantity of random damage event are relatively large
Small MDEE	Both physical scale and quantity of random damage event are relatively small	Large quantity of random damage events with low event energy

work, we focused on the pre-yield and yield random damage events, even though there are some interesting results in the post-yield stage as well.

We used two parameters to quantify the random events in the pre-yield stage: (1) the intensity of random damage events (IRDE), which is a measure of the damage events per unit interface bonding area; and (2) the mean damage event energy (MDEE), which is a quantity that is known to be directly proportional to the physical size and the magnitude of damage events in a material [26, 27]. We will use the combination of IRDE and MDEE to reveal the characteristics of random damage that occurred at the interface (Table 1).

2.3 Generation and characterization of debris particles

To collect the debris particles at the interface of a test specimen, we designed and fabricated a fixture which created fretting (longitudinal motion of up to 1 mm), through the action of a 600 mm-long lever arm (Fig. 2). This amount of fretting movement is within the range that has been estimated to occur in vivo in cemented THRs. In fact, recent measurement of stem-cement micromotion from en bloc retrieved cemented THRs show that micromotion can range from very small (0.6 microns) for well-fixed implants to 0.83 mm for loose ones (Mann KA. Personal communication, July 2009.). This arm was designed with a cavity to house the test specimen, a provision for the manual application of a shear force to break the interfacial bond first, and a provision for producing repetitive shear motion at a frequency of 1 Hz about the pivoting pin of the fixture. When testing the specimens, we used a quasi-static direct shear force corresponding to a normal stress of ~3 MPa according to an estimated working stress range at the stem-implant interface in a cemented THR [28]. Each test was repeated three times. All tests were performed in ambient laboratory air (21 ± 1°C). The protocol used to collect the debris particles was as follows: under a combined normal and shear stress, break the bond first, and then test for ten cycles at an angle that generates reciprocating motion of 1 mm at the free end of the interface (Fig. 2). The sliding contact surfaces were then separated and the debris particles collected using scanning electron microscopy (SEM) adhesive stubs. The debris particles were collected from the stem surface at the distance between ~0 displacement near the pivoting pin and maximal displacement (1 mm) at the free end of the interface. (From this study, it suggests that the next step is to collect debris particles at different distances that represent various level of post debonding motion). The stubs were then coated with a 10 nm layer of Au–Pd to prevent electron beam charging in the microscope. Debris particles were also collected and examined after 100 loading cycles. The shape and size of the debris particles after ten loading cycles and after 100 loading cycles were then estimated with the aid of scanning electron micrographs. We conducted these tests with only satin-finish and grit-blasted interface specimens because stems with these finishes are widely used in cemented THRs.

All statistical tests were conducted using ANOVA.

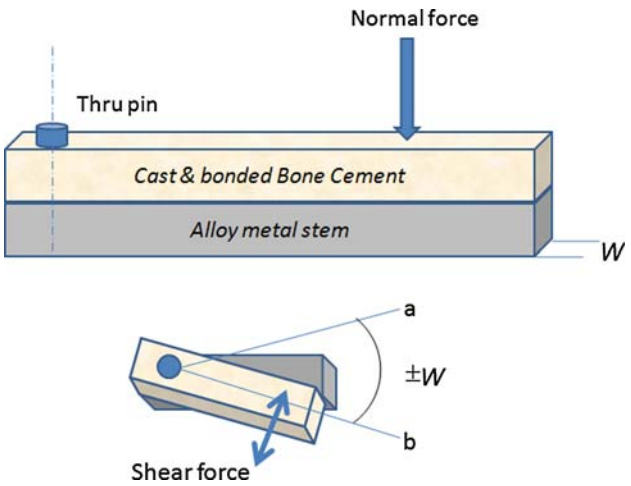

Fig. 2 A schematic drawing of the principles of the setup used for generating the debris particles at the interface of the specimens, under direct shear load

3 Results

3.1 Surface roughness of CoCr bars in test specimens

The surface roughness (R_a) for the CoCr alloy bars in the satin-finish, grit-blasted, and plasma-sprayed specimens were 0.85 ± 0.03, 3.95 ± 0.15, and 9.29 ± 0.29 μm,

respectively. The R_a magnitudes were significantly different for the three groups ($p < 0.0001$).

3.2 Patterns of evolution of random events

Typical temporal variations of the load and the corresponding random damage events in the three study groups are shown in Fig. 3. Note that the dots are the acoustic signals, whose amplitudes are indicated on the right-hand vertical axis.

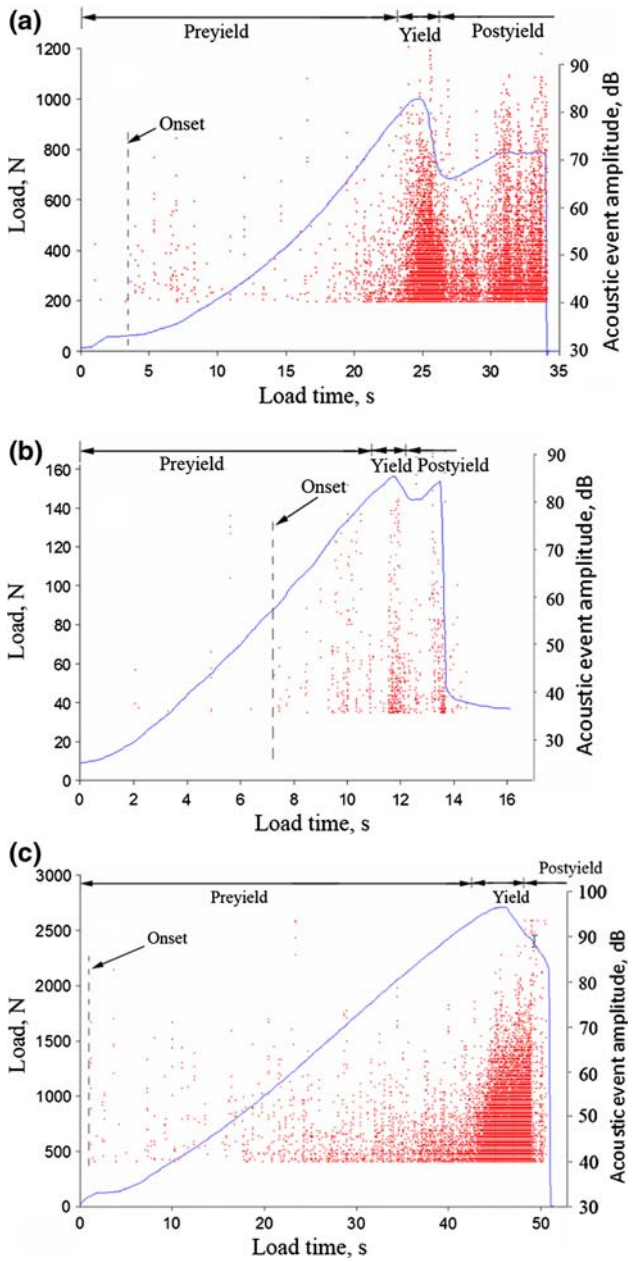

Fig. 3 Typical loading patterns in the pre-yield, yield, and post-yield stages, as identified by AE, and the point of onset of random damage events: **a** grit-blasted specimen, **b** satin-finish specimen, and **c** plasma-sprayed specimen, (Note the change of load scale for each group)

3.3 Measurements of random damage events

For specimens in each of the study groups, there were a large number of random damage events detected at each loading stage (Table 2). IRDE for the plasma-sprayed was significantly greater than that for the other two groups ($p < 0.0001$ in both cases). IRDE for the grit-blasted group was higher than that for the satin-finish group, though not significantly so ($p = 0.2986$). MDEE for the satin-finish group was significantly greater than that for the grit-blasted and the plasma sprayed groups ($p = 0.0008$ and 0.0015, respectively). MDEE for the grit-blasted and the plasma-sprayed groups were not significantly different ($p = 0.9859$). However, there were significant differences between satin-finish group and the other two groups for both the IRDE and MDEE in the yield stage ($p < 0.0001$).

3.4 Stress and acoustic emission parameters

The difference in τ_s for the specimens in the three study groups (Table 3) was significant ($p < 0.0001$). The difference in τ_o between the grit-blasted and plasma-sprayed groups was not significant ($p = 0.7268$), but the value for each of these groups was significantly greater than that for the satin-finish group ($p = 0.0408$ and 0.0218, respectively). The difference in SR between the satin-finish and grit-blasted groups was not significant ($p = 0.0579$), but the value for each of these groups was significantly greater than that for the plasma-sprayed group ($p = 0.0004$ and 0.0340, respectively).

3.5 Correlations between R_a, SR, and IRDE

Surprisingly, the stress ratio (SR) decreased linearly with increase in R_a although the correlation was weak ($R^2 = 0.383$, $p < 0.0001$, Fig. 4a). In contrast, there was a strong exponential increase of IRDE with increasing R_a ($R^2 = 0.729$, $p < 0.0001$, Fig. 4b). Note that in the range 8 μm < Ra < to 10 μm, the value of IRDE increased substantially (Fig. 4b).

3.6 Morphological features of interfaces

The morphological features of the stem surfaces of the interfaces after the shear tests are presented in Fig. 5. The satin-finish stem surface is shown in Fig. 5a. It is mainly the metal surface (in light color) without any obvious residue of broken cement, except for one dark area (indicated by an arrow), which was a surface defect. For a grit-blasted specimen, we find a roughened cement surface

Table 2 Number of random damage events, intensity of random damage event (IRDE), and mean damage event energy (MDEE) in the pre-yield and yield loading stages

Surface finish	Microcracks	Pre-yield stage	Yield stage
Satin-finish	Total no. of random damage events	642 ± 304	1036 ± 310
	IRDE [no./mm^2]	1.0 ± 0.43	1.8 ± 0.54
	MDEE [eu/event]	112.8 ± 36.17	323.3 ± 74.40
Grit-blasted	Total no. of random damage events	1519 ± 397	2624 ± 235
	IRDE [no./mm^2]	3.2 ± 0.73	4.6 ± 0.41
	MDEE [eu/event]	8.4 ± 1.13	69.2 ± 18.42
Plasma-sprayed	Total no. of random damage events	5436 ± 930	5028 ± 581
	IRDE [no./mm^2]	15.7 ± 2.82	13.9 ± 1.76
	MDEE [eu/event]	7.9 ± 1.46	127.8 ± 30.63

Table 3 Apparent interface shear strength, microcrack activity onset stress, and stress ratio for the three study groups

Surface finish	Interface shear strength, τ_s (MPa)	Onset stress, τ_o (MPa)	Stress ratio ($=\tau_o/\tau_s$) (%)
Satin-finish	0.377 ± 0.056	0.108 ± 0.031	25.842 ± 6.229
Grit-blasted	1.915 ± 0.107	0.273 ± 0.034	15.200 ± 2.335
Plasma-sprayed	9.480 ± 0.317	0.300 ± 0.085	3.237 ± 0.882

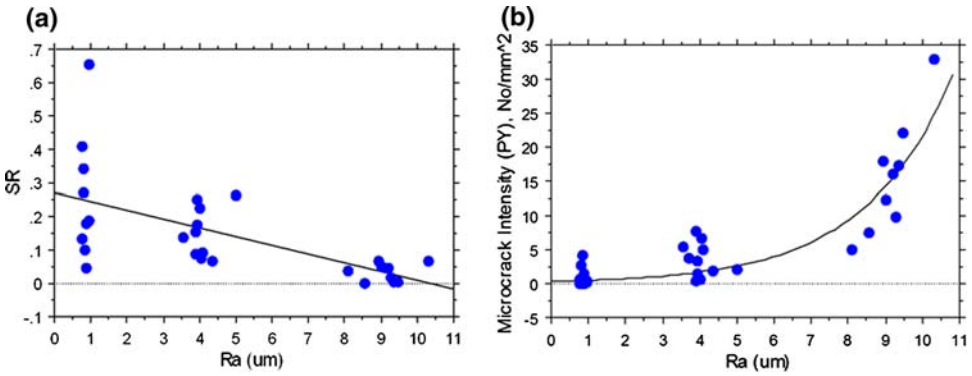

Fig. 4 **a** Correlation obtained between SR and R_a was: $SR = 0.27 - 0.026 \times R_a (R^2 = 0.383,\ p < 0.0001)$; **b** correlation obtained between IRDE and R_a was: $IRDE = 0.316e^{0.423 \times R_a} (R^2 = 0.729,\ p < 0.0001)$

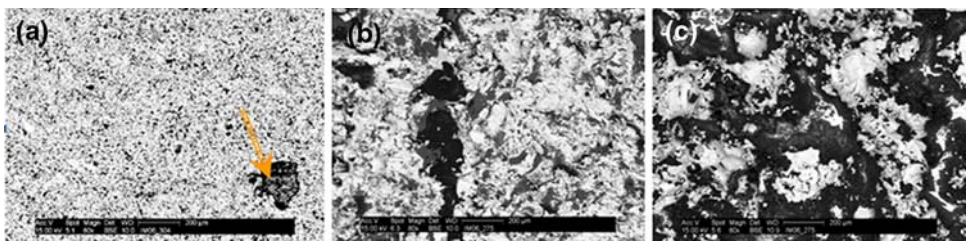

Fig. 5 Morphological features of the surfaces of the interfaces in test specimens after the shear tests. **a** Alloy side of the interface in satin-finish specimen. There is only one *black spot* on the surface (indicated by an *arrow*); **b** cement side of the interface in a grit-blasted specimen; **c** cement side of the interface in a plasma-sprayed specimen. In **b** and **c**, the *light* and *dark* areas are the metal and the broken interlocked cement, respectively

characterized by fragments and surface irregularities (Fig. 5b), a result of stem-cement debonding and fracture-interlocked cement (indicated by the dark areas). Dark areas (broken interlocked bone cement) are the dominant features in the case of a plasma-sprayed specimen (Fig. 5c). The observations of the transverse cross sections

Table 4 Sizes of debris particles generated at the interface of test specimens after 10 and 100 cycles of repetitive shear load

Surface finish	10 cycles [μm]	100 cycles [μm]
Satin-finish[a]	150 × 20	150 × 50
Grit-blasted[b]	~50	~20

[a] These measurements are length × diameter

[b] The measurement is diameter

of the cement did not yield any distinguishable random damage events that appeared to be due to the failures at the interface that migrated into the bulk of cement mantle.

3.7 Characteristics of debris particles

Since satin finish and grit blasted interfaces are the ones that are currently in use, we focused on these two groups only. Regardless of the study groups, the debris particles produced at the interface in a test specimen were entirely bone cement particles, leading to the conclusion that the interfacial bond strength is limited by the bond strength of the cement. The sizes of the cement debris particles are summarized in Table 4. For the satin-finish specimens, (1) after ten loading cycles, the debris particles were cylindrical in shape (~150 μm long by ~20 μm in diameter), a result of rolling-up flat debris sheets and loosened cement particles; and (2) when the number of loading cycles increased to 100, agglomerations of smaller rolled-up particles with increased diameter of ~50 μm were produced (see the top two micrographs in Fig. 6a). In contrast, for the grit-blasted specimen, (1) smaller debris particles (<50 μm)—including the complete removal of some cement beads—were produced after ten cycles; and (2) when the number of cycles was increased to 100, the particles were further fragmented to be ~25 μm (see the bottom micrographs in Fig. 6a). There were no rolled-up debris particles obtained from grit-blasted specimens.

We noticed that, after debonding, the resistance to small-angle reciprocating motion was essentially the same for the satin-finished and the grit-blast specimens. This resistance is schematically depicted in Fig. 6b. Noteworthy is the residual unsheared bone cement, which fills the surface cavities, with the thickness being determined by the height of the metal surface asperities. A similar phenomenon was noticed in different pairs of interface specimens in our previous study [28].

4 Discussion

The acoustic signals revealed that, in each specimen in each of the study groups, random damage events occurred at surprisingly low stress (0.1–0.3 MPa). Shear stresses at the stem-cement interface of a bonded stem-cement interface in a THR have been estimated to be 1–3 MPa [29]; thus, the present results suggest that, in vivo, there is a high probability that random damage would occur at the stem-cement interface. Because local fracture/debonding are the most likely causes that could produce debris particles in the early loading stages, our technique to quantify the associated acoustic events is a unique way to reveal the production of debris at the stem-cement interface. The combination of significantly larger IRDE and small MDEE values for the plasma-sprayed and the grit-blasted specimens compared to the satin-finish ones (Table 2) suggests that there would be a much higher probability for generation of random damage events in small physical scales. These events are eventually attributed to the production of large quantity of small debris particles at the stem-cement interface. Together with Fig. 5, our data suggest that the

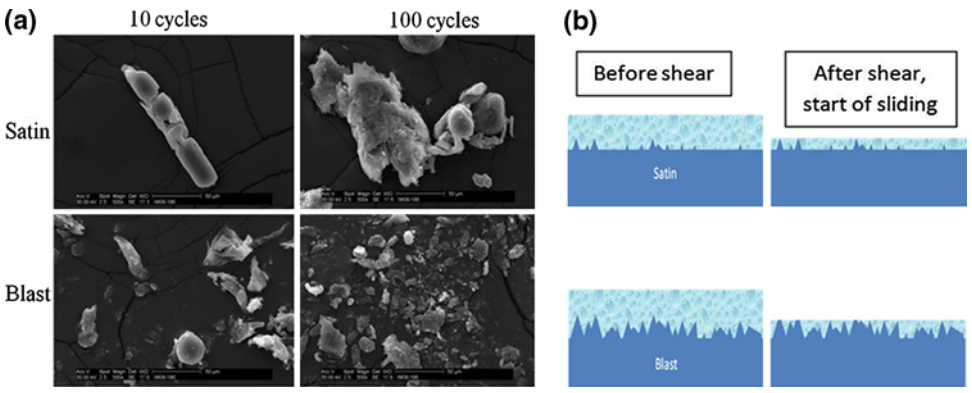

Fig. 6 **a** Micrographs of bone cement wear debris from the surfaces of satin-finish and grit-blasted specimens after 10 and 100 cycles of small-angle reciprocating motion (500× magnification in all cases); **b** a schematic depiction of the as-cast and bonded bone cement/metal interface for satin-finish and grit-blasted specimens. 'Before shear' is the as-cast condition and 'after shear' is the sheared and debonded starting point, from which additional rubbing cycles accumulate

dominant failure mechanism at rough stem interface is the breakage of interlocked cement fragments. The combination of small IRDE and large MDEE values for the satin finish interface indicates that the dominant failure mechanism at this interface is debonding.

There have been contradicting reports regarding the relative longevities of cemented THRs having grit-blasted versus satin-finish stem [17–21, 23]. We contend that our results for the random damage parameters (IRDE and MDEE) for the grit-blasted specimens may contribute to a resolution of this controversy. We note that IRDE for the grit-blasted specimens was significantly higher than for satin-finish specimens while the trend for the MDEE results is the reverse. Taken together, these results suggest a significantly higher probability for debris particles generation at the interface in grit-blasted specimens than in satin-finish ones.

We recognize some limitations of our study. First, the loading was quasi-static. Although, during most daily activities, the stem-cement interface is subject to cyclical loading, for some cases, such as sitting, the loading experienced is quasi-static. Because we found that random damage events occur at very low apparent shear stresses, these damage events are anticipated to occur even in early fatigue loading stages. Second, the tests were carried out in air rather than in, say, phosphate buffered saline (PBS), at 37°C. We do not anticipate that the trends seen in the present work would be different if the tests are conducted in PBS, at 37°C. Third, we used rectangular stem and cement layers, whereas, the shape of the stem-cement construct is complex. From the generation of random damage point of view, construct geometry is unlikely to have a marked effect on the trends seen in our results. Lastly, we collected the debris particles under dry conditions. However, according to the principles of friction, dry friction is the worst-case scenario [30, 31].

In conclusion, the results support both study hypotheses. The significance and implication of this work are that there exist significant differences in even a very basic simple stem-cement interface model, and these differences suggest that satin-finish stems are desirable.

Acknowledgments The project described was supported by Grant Number AR051119 from NIH/NIAMS. The authors would like to thank Mr. Bin Zhang and Dr. Jihui Li for assisting the experimental work.

References

1. Wang JS, Taylor M, Flivik G, Lidgren L. Factors affecting the static shear strength of the prosthetic stem–bone cement interface. J Mater Sci: Mater Med. 2003;14:55–61.
2. Mann KA, Damron LA, Miller MA, Race A, Clarke MT, Cleary RJ. Stem-cement porosity may explain early loosening of cemented femoral hip components: experimental-computational in vitro study. J Orthop Res. 2007;25(3):340–50.
3. Bishop NE, Ferguson S, Tepic S. Porosity reduction in bone cement at the cement–stem interface. J Bone Joint Surg. 1996;78-B:349–57.
4. Race A, Miller MA, Ayers DC, Cleary RJ, Mann KA. The influence of surface roughness on stem–cement gaps. J Bone Jnt Surg. 2002;84B:1199–204.
5. Race A, Miller MA, Clarke MT, Mann KA. Cement-implant interface gaps explain the poor results of CMW3 for femoral stem fixation: a cadaver study of migration, fatigue and mantle morphology. Acta Orthop. 2005;76:679–87.
6. Wang JS, Franzen H, Lidgren L. Interface gap after implantation of a cemented femoral stem in pigs. Acta Ortho Scand. 1999;70:234–9.
7. Damron LA, Kim DG, Mann KA. Fatigue debonding of the roughened stem-cement interface: effects of surface roughness and stem heating conditions. J Biomed Mater Res Part B: Appl Biomater. 2006;78B:181–8.
8. Dall DM, Miles AW, Juby G. Accelerated polymerization of acrylic bone cement using preheated implants. Clin Orthop Relat Res. 1986;211:148–50.
9. Mann KA, Damron LA, Race A, Ayers DC. Early cementing does not increase debonds energy of grit blasted interfaces. J Orthop Res. 2004;22:822–7.
10. Crowninshield RD, Jennings JD, Laurent ML, Maloney WJ. Cemented femoral component surface finish mechanics. Clin Orthop Relat Res. 1998;355:90–102.
11. Barb W, Park JB, Kenner GH, von Recum AF. Intramedullary fixation of artificial hip joints with bone cement-precoated implants. I. Interfacial strengths. J Biomed Mater Res. 1982;16:447–58.
12. Bundy KJ, Penn RW. The effect of surface preparation on metal/bone cement interfacial strength. J Biomed Mater Res. 1987;21:773–805.
13. Davies JP, Singer G, Harris WH. The effect of a thin coating of polymethylmethacrylate on the torsional fatigue strength of the cement-metal interface. J Appl Biomater. 1992;3:45–9.
14. Ahmed AM, Raab S, Miller JE. Metal/cement interface strength in cemented stem fixation. J Orthop Res. 1984;2:105–18.
15. Raab S, Ahmed AM, Provan JW. The quasistatic and fatigue performance of the implant/bone-cement interface. J Biomed Mater Res. 1981;15:159–82.
16. Mann KA, Edidin AA, Ordway NR, Manley MT. Fracture toughness of CoCr alloy-PMMA cement interface. J Biomed Mater Res. 1997;38:211–9.
17. Collis DK, Mohler CG. Loosening rates and bone lysis with rough finished and polished stems. Clin Orthop Rel Res. 1998;355:113–22.
18. Della Valle AMG, Zoppi A, Peterson MGE, Salvati EA. A rough surface finish affects the clinical and radiographic performance of a modern cemented femoral stem. Clin Orthop Relat Res. 2005;436:158–63.
19. Ong A, Wong KL, Lai M, Garino JP, Steinberg ME. Early failure of precoated femoral components in primary total hip arthroplasty. J Bone Joint Surg. 2002;84-A:786–92.
20. Della Valle AG, Rana A, Nestor B, Bostrom M, Westrich G, Salvati EA. Metallic shedding, surface finish changes, and extensive femoral osteolysis in the loose Spectron EF stem. Clin Orthop Relat Res. 2006;442:165–70.
21. Rasquinha VJ, Ranawat CS, Dua V, Ranawat AS, Rodriguez JA. A prospective, randomized, double-blind study of smooth versus rough stems using cement fixation: minimum 5-year follow-up. J Arthroplasty. 2004;19(Suppl 2):2–9.
22. Vail TP, Goetz D, Tanzer M, Fisher DA, Mohler CG, Callaghan JJ. A prospective randomized trial of cemented femoral components

with polished versus grit-blasted surface finish and identical stem geometry. J Arthroplasty. 2003;18(Suppl 1):95–102.
23. Verdonschot N, Tanck E, Huiskes R. Effects of prosthesis surface roughness on the failure process of cemented tip implants after stem-cement debonding. J Biomed Mater Res. 1998;42:554–9.
24. Beksac B, Taveras BS, Gonzales DV, Salvati EA. Surface finish mechanics explain different clinical survivorship of cemented femoral stems for total hip arthroplasty. J Long-Term Eff Med. 2006;16(6):407–22.
25. Heuer DA, Mann KA. Fatigue fracture of the stem-cement interface with a clamped cantilever beam test. J Biomech Eng. 2000;122:647–51.
26. Qi G, Li J, Mann KA, Mouchon WP, Hamstad MA, Salehi A, et al. 3D real time methodology monitoring cement failures in THA. J Biomed Mater Res A. 2004;71:391–402.
27. Qi G. Attenuation of acoustic emission body waves in acrylic bone cement and synthetic bone using wavelet time-scale analysis. J Biomed Mater Res. 2000;521:148–56.
28. Thota S. Acoustic emission detection of X-force horizontal conveyer bearings and sliding material pairs. MS thesis. The University of Memphis; 2008.
29. Chang PB, Mann KA, Bartel DL. Cemented femoral stem performance. Effects of proximal bonding, geometry, and neck length. Clin Orthop Relat Res. 1998;355:57–69.
30. Kimura Y, Sugimura J. Microgeometry of sliding surfaces and wear particles in lubricated contact. Wear. 1984;100:33–45.
31. Waterhouse RB. Fretting corrosion. NY: Pergamon Press; 1972.